frontiers | Frontiers in Earth Science

TYPE Original Research
PUBLISHED 27 September 2022
DOI 10.3389/feart.2022.1024483

OPEN ACCESS

EDITED BY
Junjian Zhang,
Shandong University of Science and Technology, China

REVIEWED BY
Run Chen,
China University of Mining and Technology, China
Gaofeng Liu,
Henan Polytechnic University, China

*CORRESPONDENCE
Chengtao Yang,
byctat@163.com

SPECIALTY SECTION
This article was submitted to Economic Geology,
a section of the journal
Frontiers in Earth Science

RECEIVED 21 August 2022
ACCEPTED 07 September 2022
PUBLISHED 27 September 2022

CITATION
Liu J, Song Z, Yang C, Li B, Ren J and Xiao M (2022), True triaxial experimental study on the influence of axial pressure on coal permeability.
Front. Earth Sci. 10:1024483.
doi: 10.3389/feart.2022.1024483

True triaxial experimental study on the influence of axial pressure on coal permeability

Jianbao Liu[1,2], Zhimin Song[1,2,3], Chengtao Yang[4]*, Bing Li[1], Jiangang Ren[1] and Ming Xiao[1]

[1]Henan University of Engineering, Zhengzhou, China, [2]Henan Polytechnic University, Jiaozuo, China, [3]North China University of Water Resources and Electric Power, Zhengzhou, China, [4]Henan Energy and Chemical Industry Group Research Institute Co., Ltd, Zhengzhou, China

The permeability of coal is a key parameter affecting coal and gas outbursts and coal seam gas drainage. The permeability is clearly affected by geo-stress. In this study, the influence of the axial pressure on the permeability of the coal seam was studied using a self-developed true triaxial stress permeability experimental device to set fixed gas and confining pressures, and to change the magnitude of the axial pressure. The experimental results show a polynomial relationship between the axial pressure and the permeability of the coal seam. With an increase in axial pressure, the permeability initially decreased slightly and then increased gradually. When the axial pressure exceeded 30 MPa, the permeability of the coal seam sharply increased. This may be due to plastic deformation of the coal seam under a large axial pressure, resulting in new fractures and significantly improving the permeability of the coal seam. Using the COMSOL numerical simulation software, the effect of *in situ* stress on the coal seam gas drainage efficiency was calculated by comprehensively considering the adsorption/desorption, diffusion, and seepage of gas. The calculation results show that with an increase in the axial pressure, the gas drainage efficiency of the coal seam increases continuously. As the axial pressure increased from 5 to 30 MPa, the gas drainage efficiency increased to 2–3 times that of the original value.

KEYWORDS

true triaxial seepage experiment, anthracite, permeability, numerical simulation, drainage efficiency

Introduction

The risk of coal and gas outbursts in high-gas mines, and coal and gas outburst mines, increases with an increase in coal mining depth. Simultaneously, different structural phenomena such as folds and small faults are encountered in the coal mining process. These structures form stress concentration areas, which are the ideal areas for gas occurrence and coal and gas outbursts (Meng and Li, 2017; Shi et al., 2018; Yan et al., 2019; Lv et al., 2022; Tatyana et al., 2022; Wang et al., 2018). This phenomenon is caused by the distribution of *in situ* stress having an impact on the permeability of coal seams, which reduces the permeability of local coal seams and forms

gas accumulation zones (Guo et al., 2019; Lin et al., 2022; Liu et al., 2022). By studying permeability change laws in Permian coal reservoirs, it was found that the link between the development characteristics of natural fractures and the current *in situ* stress state has an important control effect on the permeability of Permian coal reservoirs in eastern Yunnan and western Guizhou (Ju et al., 2022). Therefore, studying the change law of coal and rock permeability under stress can reduce the occurrence of gas accidents in coal mining and improve the efficiency of gas drainage.

Previous studies investigated the relationship between axial pressure and permeability, albeit with different interpretations (Chao et al., 2019; Cheng et al., 2022; Luo et al., 2022). There are three main viewpoints regarding coal permeability as it relates to increased axial pressure: decrease permeability, increased permeability, and an initial decrease in permeability followed by an increase. A variety of fitting structures have also been proposed for the relationship model between axial pressure and coal permeability (Connell et al., 2010; Rong et al., 2018; Zhou et al., 2019; Liu and Yu, 2022; Wang et al., 2022). The first point of view is that when gas and confining pressures are constant, the permeability of coal samples decrease exponentially with an increase in axial pressure (Xue et al., 2020; Li B. B et al., 2020). A study on the permeability of hard and soft coal by Sun et al. (2016) found that the change in axial pressure and permeability of hard coal conforms to the change law of linear decrease, and the influence of axial pressure on the permeability of soft coal is greater than that of hard coal. The second point of view is that the permeability of coal and rock mass in the pre- and post-peak stages show an exponential growth trend with stress; however, there are obvious differences in the growth amount between the two (Xue et al., 2017). The third point of view is that the permeability decreases first and then increases with the type of coal sample. This means that the permeability of gas bearing coal shows a "V" shape change pattern (Zhao, 2018; Li H. G et al., 2020). At the initial stage of loading where pore compression and elastic deformation occurs, the pores and fractures in the coal were gradually compacted, decreasing the permeability of the coal sample. In the plastic deformation stage, owing to an increase in axial stress, the fractures in the coal expand, the permeability of the coal sample increases, and the acoustic emission activity intensity increases and reaches its peak (Xie et al., 2016; Meng et al., 2020; Bai et al., 2021; Zhu et al., 2021). Through the triaxial compression of compacted clay, Wang et al. (2020) found that when the sample's confining pressure was greater than the pre-consolidation pressure, the sample always showed volume shrinkage and became denser during triaxial compression. Therefore, the permeability coefficient decreased with an increase in the axial strain and subsequently stabilized. When the sample's confining pressure is much less than the pre-consolidation pressure, a concentrated shear band is produced, which is unfavorable for seepage. The concentrated shear band became the seepage channel, and the axial permeability coefficient of the sample increased significantly with increasing axial strain.

There is also previous knowledge on the causes of permeability change (Li J. Q et al., 2020; Xue et al., 2021). Through an unloading experimental study on coal permeability, it is believed that the expansion of the original fracture and the generation of a new fracture causes the sudden increase in the permeability of the unloaded coal body (Cheng et al., 2014; Wang et al., 2021). The development law of coal sample fractures is related to loading and unloading rates (Jiang et al., 2020). The coal gradually develops from multiple macrofractures to a single macrofracture surface with an increase in the loading and unloading rate ratio, resulting in structural failure.

In this study, the change law of coal seam permeability with axial pressure was studied through the triaxial stress permeability test device under the context of fixed gas and confining pressures, and the influence of vertical formation stress on gas drainage efficiency was calculated using the COMSOL numerical analysis software.

Sample and experimental devices

Sample

The experimental sample was obtained from the Xiyang mining area in Shanxi Province. Large original coal samples with a relatively good integrity were collected from the coal mining face. The coal samples were packed, sealed, and transported to the laboratory. After cutting and grinding, the samples were processed into 100 × 100 × 100 mm cubes. The industrial analysis of coal is the main index used to understand the characteristics of coal quality and the basis for evaluating coal quality. The industrial analysis data of the coal samples measured according to GB/T212-2008 are shown in Table 1. The coal sample was anthracite, with a fixed carbon content of 72.15%.

A microscope with transmission light and reflection fluorescence functions was used to obtain quantitative statistics on the percentage content of each maceral in coal using the number point method. To determine the type of organic matter, a type index was calculated according to the different weighting coefficients of each maceral. The macerals of the coal mainly included exinite, vitrinite, and inertinite. The maceral data of the coal samples, measured according to GB/T8899-2013, are listed in Table 1. The vitrinite content of the coal sample was 82.81%.

Experimental devices

Experiments were performed using a self-developed true triaxial stress permeability test device (Figures 1, 2). The experimental equipment can complete the experimental research on gas permeability in an underground reservoir environment (triaxial pressure and temperature), and provide necessary technical support and basic scientific research data for gas disaster prevention and gas drainage in

TABLE 1 Industrial analysis and microstructure of the coal sample.

Coal types	Industrial analysis				Microstructure		
	M_{ad}/%	A_d/%	V_{daf}/%	*FCad*/%	Exinite/%	Vitrinite/%	Inertinite/%
WY	2.43	16.67	8.75	72.15	0.96	82.81	16.23

Note: M_{ad} is moisture on an air-dry basis, A_d is ash on a dry basis, V_{daf} is volatile matter on a dry ash-free basis, *and* FC_{ad}, is carbon on an air-dry basis.

FIGURE 1
Overall diagram of experimental device.

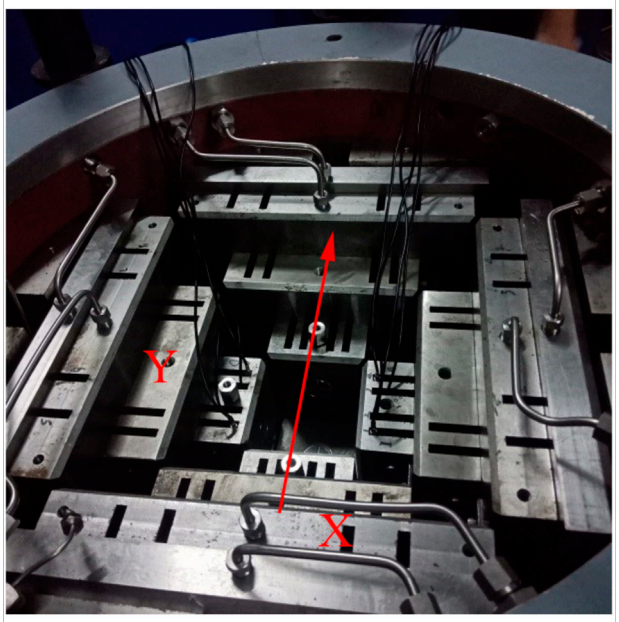

FIGURE 2
Core part of gripper. Note: The arrow stands for the gas seepage direction.

coal mines. The technical parameters of the equipment were as follows: 1) core size of 100 × 100 × 100 mm (optional sample size included 200 × 200 × 200 mm and 300 × 300 × 300 mm), a 100 × 100 × 100 mm sample was selected; 2) the maximum hydraulic pressure in the X-, Y-, and *Z*-axes of the three-axis hydraulic pressure is 40 MPa, and the control accuracy is ±0.1 MPa; 3) the gas permeability measurement range is 0.001–1,000 mD.

At home and abroad, silicone sleeves are mainly used to seal the edges of samples to prevent gas leakage during seepage. However, during the experiment, it was found that when the axial pressure was high, the silicone sleeve was more likely to be cut off. The experiment proves that the copper sleeve can not only ensure the sealing effect but also has a specific strength, strong pressure resistance and shear resistance, and that its sealing effect is better than that of the silicone sleeve. To further ensure the sealing effect, the copper sleeve was coated with epoxy resin.

Experimental results and discussions

Fracture development characteristics

The bedding plane of the experimental coal sample was placed horizontally. The two sides of the coal sample were marked as the X and Y planes, respectively, and the top surface was marked as the Z plane. The X planes are the planes through which the gas passes, and the Z planes are parallel to the bedding plane. The inlet gas pressure was set as 1.8 MPa. When the *x*-axis stress was set to 30 MPa, the *y*-axis stress was 20 MPa, and the x- and *y*-axis stresses remained unchanged. The *z*-axis stress was set to 5 MPa, 10 MPa, 15 MPa, 20 MPa, 25 MPa, 30 MPa, and 35 MPa (Figure 3) to study the influence of axial pressure change on permeability. After the experiment, the coal sample was taken out, and photographs were taken to observe the damage to the coal sample (Figure 4–6).

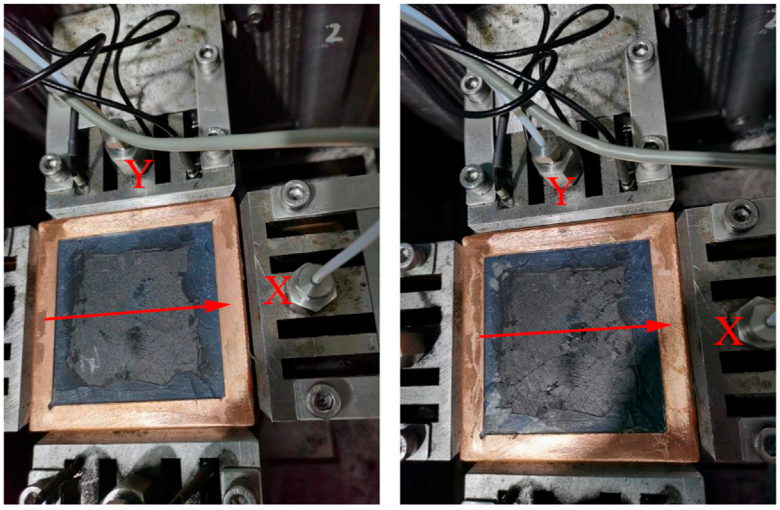

FIGURE 3
Coal sample before (left) and after (right) an axial compression permeability experiment. Note: The arrow stands for the gas seepage direction.

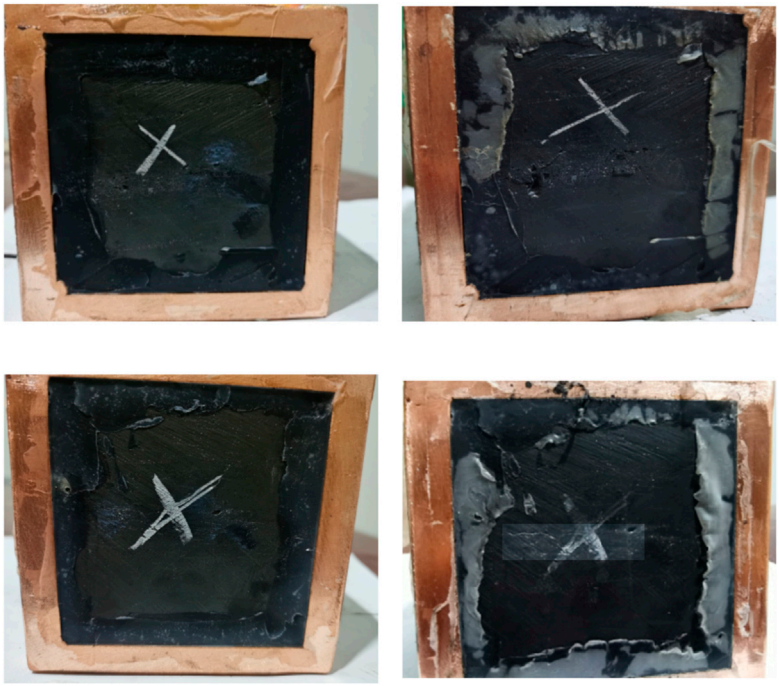

FIGURE 4
Comparison of the X plane before (left) and after (right) the experiment. Note: The fractures are highlighted with transparent frames. Fractures parallel to the bedding plane were formed.

The *in situ* stress has strong directionality, including mainly two horizontal stresses (σ_x and σ_y) and vertical stress (σ_z). In a formation where the natural fracture is not developed, the fracture shape depends on the three-dimensional stress state. According to the principle of minimum principal stress, fracture always occurs in the direction with the weakest strength and

FIGURE 5
Comparison of the Y plane before (left) and after (right) the experiment. Note: The fractures are highlighted with transparent frames. Fracture system perpendicular to the bedding plane and parallel to the bedding plane were formed.

smallest resistance. In other words, the rock fracture surface is perpendicular to the direction of the minimum principal stress (Barnett et al., 2015). Horizontal fractures tend to occur when the horizontal stress is greater than the vertical stress. On the same vein, vertical fractures are easily generated when the vertical stress is greater than the horizontal stress. The relationship between the stress and fractures is shown in Figure 7.

Therefore, in the process of σ_z change, the coal samples formed fractures in different directions. When σ_z was 5–20 MPa, the minimum principal stress was σ_z, and fractures perpendicular to the *z*-axis were formed, parallel to the bedding plane. The difference between the maximum and minimum principal stresses at this stage was 10–25 MPa. The formed fracture was evident on the Y plane of the sample. When σ_z is between 20 and 30 MPa and 30 and 35 MPa, the minimum principal stress is still σ_y. However, the maximum principal stress changes from σ_x to σ_z, and the intermediate principal stress changes from σ_z to σ_x. The stress difference increases from 10 MPa to 10–15 MPa, and fractures are formed on the Y and Z planes of the coal sample. However, the fractures are not well-developed on the X plane. This may be related to the heterogeneity of the coal samples and local development of microcracks. Under the action of triaxial stress, fractures develop along the direction of the microcracks, which are associated with macroscopic fractures. These provide channels for methane seepage and increase the permeability of the coal seams.

Variation characteristics of permeability

When the *z*-axis stress was low (less than 30 MPa), the permeability changed slightly with the change in axial pressure. However, when the axial pressure was high (more than 30 MPa), the permeability increased significantly. To further study the relationship between the axial pressure and initial permeability, as well as the permeability change, exponential function fitting, power function fitting, and polynomial fitting were performed on the experimental data using MATLAB. The fitting results are shown in Figure 8, Figure 9, and Figure 10 and Table 2. The best fitting model was the polynomial fitting, and the sum of the residual squares is one order of magnitude lower than the exponential and power functions. By analyzing the fitting curve, it can be found that with an increase in axial pressure,

FIGURE 6
Comparison of the Z plane before (left) and after (right) the experiment. Note: The fractures are highlighted with transparent frames. Fractures develop along the direction of the microcracks.

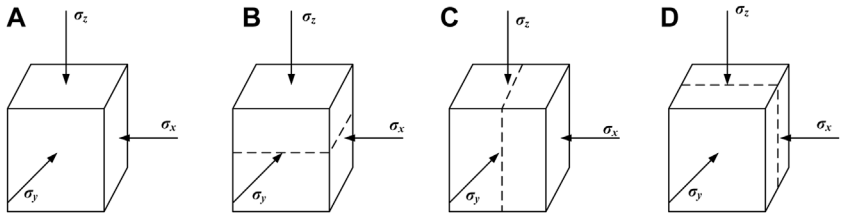

FIGURE 7
Relationship between stress and fracture morphology.**(A)** Three-dimensional stress state. **(B)** When σ_z is the minimum principal stress, horizontal fractures are formed. **(C)** When σ_x is the minimum principal stress, fractures perpendicular to σ_x are formed. **(D)** When σ_y is the minimum principal stress, fractures perpendicular to σ_y are formed.

the permeability shows a slight decrease at the stage of low axial pressure and then increases slowly. When the axial pressure exceeded 30 MPa, permeability increased sharply. This may be because the increase in the axial pressure condenses the pores and fractures of the coal sample in the initial stage; however, when the axial pressure exceeds the elastic deformation stage of the coal sample, plastic deformation begins to occur, forming new fractures, improving the permeability of the coal seam, and increasing permeability significantly.

Numerical simulation

To evaluate the influence of *in situ* stress on coal seam gas drainage efficiency, COMSOL was used to fully consider the overall process of gas adsorption/desorption, diffusion, and seepage through fluid–solid coupling analysis; a model was established for numerical analysis and calculation. Drawing from previous research results (Wang et al., 2016), the parameter settings for each module are listed in Table 3. The length and width of the model were set to 100 m, height

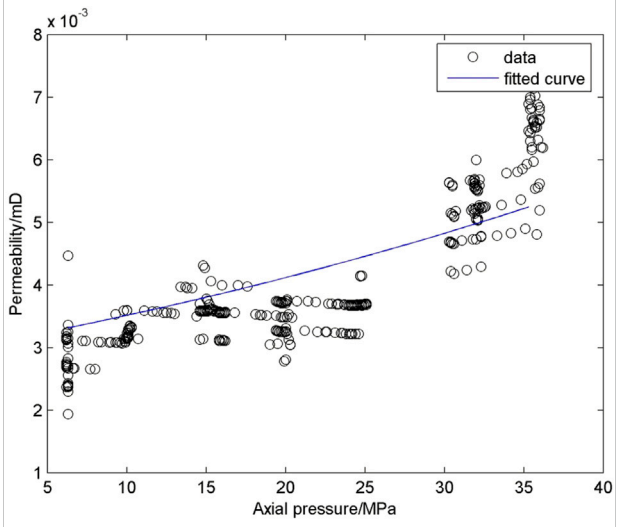

FIGURE 8
Exponential function fitting between axial pressure and permeability.

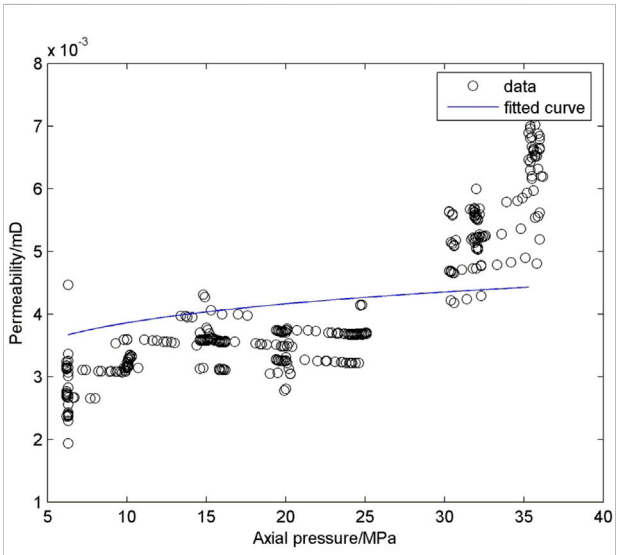

FIGURE 9
Power function fitting between axial pressure and permeability.

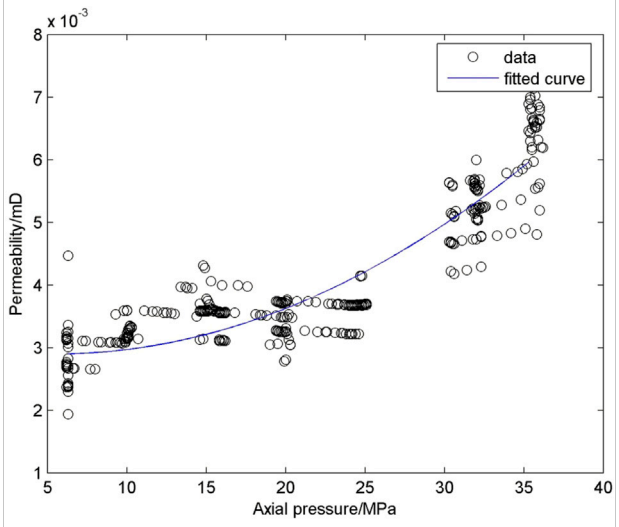

FIGURE 10
Polynomial fitting between axial pressure and permeability.

was set to 6 m, and drilling radius was set to 0.1 m. The established geometric model is shown in Figure 11.

The solid mechanics module adopts the linear elastic model and sets the left interface, front interface, and lower interface as the sliding boundary; in other words, the displacement in the normal direction is 0. The right interface was set as the pressure boundary, with a pressure of 30 MPa, simulating the *x*-axis stress in the true triaxial stress seepage experiment. The rear interface was set as the pressure interface with a pressure of 20 MPa, simulating the *y*-axis stress in the experiment. The upper boundary was set as the pressure boundary, and its stress was set to 5, 10, 15, 20, 25, and 30 MPa, simulating the stress in the *z*-axis direction perpendicular to the bedding plane of the coal seam.

The diffusion process was simulated using a general partial differential equation. In the process of gas extraction, the adsorbed gas in the coal matrix is desorbed as a mass source, so that diffusion and seepage continue. The mass exchange between the coal matrix and the fracture system can be expressed as:

$$Q = \frac{M}{tRT}(u - p). \tag{1}$$

There are both adsorbed gas and free gas in the pores of coal matrix. The total gas storage quality can be expressed as:

$$m = \frac{V_L u}{u + P_L}\rho_m \rho_g + \varphi_0 \frac{M}{RT} u. \tag{2}$$

The partial derivative of formula 2 to time is the mass exchange between coal matrix and fracture system. Therefore, the following formula can be obtained:

$$\frac{\partial m}{\partial t} = -\frac{M}{tRT}(u - p). \tag{3}$$

Then the diffusion source term f is expressed as:

TABLE 2 Comparison of fitting results of different methods.

Fitting formula	Fitting results	Sum of squares of residuals
$y = k_0 e^{ax}$	$y = 0.003e^{0.0158x}$	2.0835e-004
$y = k_0 x^a$	$y = 0.003x^{0.1093}$	4.1057e-004
$y = ax^2 + bx + k_0$	$y = 0.0001 \times (0.0343x^2 - 0.3737x) + 0.003$	9.5060e-005

Note: k_0 is the initial permeability, which was taken as 0.003 mD according to the results of the true triaxial stress seepage experiment.

TABLE 3 Numerical simulation parameters.

Parameters	Value [unit]	Descriptions
E	2,713 [MPa]	Elastic modulus of coal
ν	0.339	Poisson's ratio of coal
ρ_m	1,250 [kg/m³]	Coal seam density
ρ_g	0.717 [kg/m³]	Methane density under standard conditions
k_0	0.00315 [mD]	Initial permeability
φ_0	0.06	Initial porosity
μ	1.08E-5 [Pa·s]	Dynamic viscosity of methane
V_L	0.02 [m³/kg]	Langmuir constant (limit adsorption capacity)
P_L	1 [MPa]	Langmuir pressure
V_M	22.4 [L/mol]	Molar volume of methane under standard conditions
R	8.413,510 [J/mol/K]	Gas state constant
T	293 [K]	Sample temperature
M	16 [g/mol]	Gas molecular mass of methane
F_x	30 [MPa]	Confining pressure in X direction
F_y	20 [MPa]	Confining pressure in Y direction
F_z	5, 10, 15, 20, 25, 30 [MPa]	Axial pressure in Z direction
r	0.1 [m]	Drilling radius
p_0	1.8 [MPa]	Initial pressure
p_b	0.087 [MPa]	Pumping negative pressure
t	9.2 [d]	Adsorption time

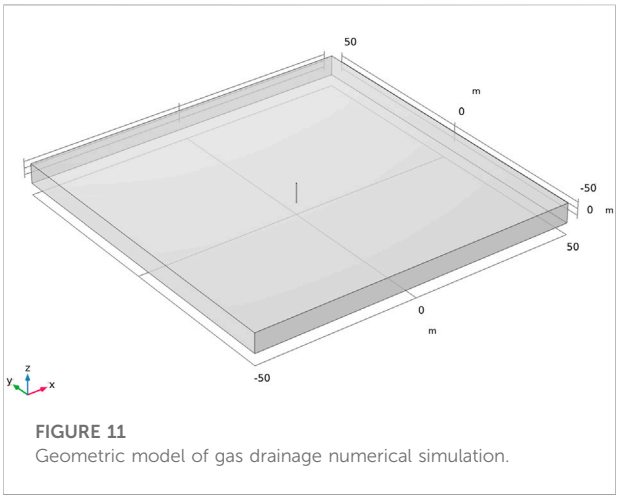

FIGURE 11
Geometric model of gas drainage numerical simulation.

$$f = \frac{\partial u}{\partial t} = -\frac{V_M (u - p)(u + P_L)^2}{tV_L RTP_L \rho_m + t\varphi_0 V_M (u + P_L)^2}, \quad (4)$$

where u represents the gas pressure in the pore and p represents the gas pressure in the fracture.

Darcy's law was adopted for the seepage model. The initial pressure of the model was set as 1.8 MPa, the conditions of four boundaries perpendicular to the bedding plane were set as the pressure boundary, the gas pressure was set as 1.8 MPa, and the pumping negative pressure of the pumping hole was set to 0.087 MPa. The permeability was taken as the fixed permeability k_0 (the axial pressure was set to 5 MPa) and the permeability k (the axial pressure was set to 10 MPa, 15 MPa, 20 MPa, 25 MPa, and 30 MPa) that changed with the axial stress.

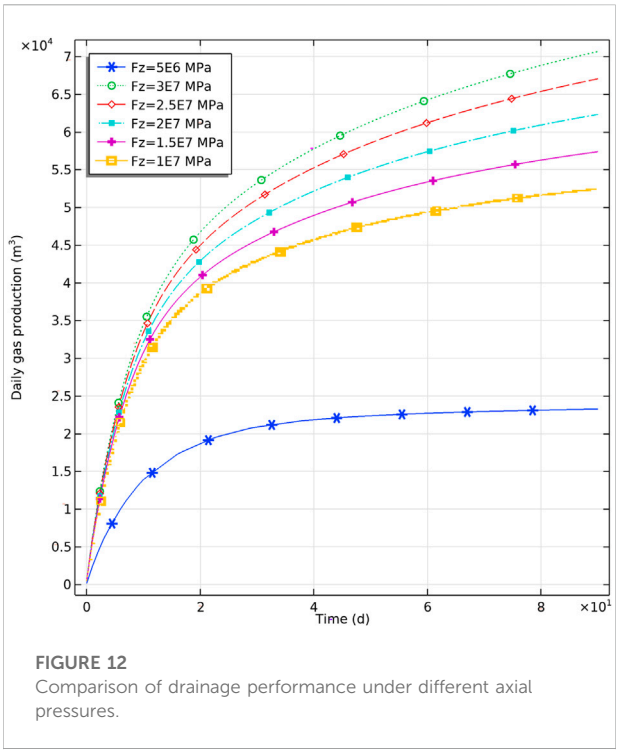

FIGURE 12
Comparison of drainage performance under different axial pressures.

The expression is as follows according to the results of the true triaxial stress seepage experiment in Table 2:

$$k = 0.0001 \times \left(0.0343\sigma_z^2 - 0.3737\sigma_z\right) + 0.003. \quad (5)$$

σ_Z is the stress in Z direction. It should be noted that here we use σ_Z replaces F_Z, because we think that on an infinitesimal element, stress can better express the influence of *in-situ* stress on permeability.

The results of the numerical simulation show that under the condition of fixed permeability, the daily gas production of boreholes maintains a high rising rate within 20 days, and the rising rate slows down in 20–40 days (Figure 12). After 40 days, the daily gas production reached equilibrium and was stable at 23,000 m^3. When the permeability varies with stress, the daily gas production of boreholes increases gradually with an increase in axial stress, and the number of days to reach equilibrium increases significantly. The daily gas production reached 52,000–70 000 m^3, which is 2–3 times that under the condition of fixed permeability. With an increase in the axial pressure, the amplification of the daily gas production decreased.

Conclusion

The results of the true triaxial stress seepage experiment with fixed confining pressure, fixed gas pressure, and axial pressure change show that with the change in axial pressure, the largest principal stress and minimum principal stress continuously change, forming fractures in different directions. The fracture surface perpendicular to the direction of the minimum principal stress was relatively developed, forming a fracture system perpendicular to the bedding plane and parallel to the bedding plane, which significantly improved the permeability of the coal sample.

Polynomial fitting was found to be the best method to fit the relationship between permeability and axial pressure through statistical processing of the experimental data with MATLAB. With an increase in axial pressure, the permeability first decreases and reaches a minimum value at approximately 5.5 MPa, which may be related to the compression of pores and fractures in the elastic deformation stage. Subsequently, it increased slowly. When the axial pressure was greater than 30 MPa, permeability increased significantly. This may be because a fracture system with vertical and parallel bedding planes was formed during the plastic deformation stage.

With an increase in axial pressure, the permeability of coal increased, and the drainage efficiency of coalbed methane increased. The daily gas production of variable permeability is 2–3 times that of fixed permeability, and the time required to reach the equilibrium drainage volume is extended.

Data availability statement

The original contributions presented in the study are included in the article/supplementary material, further inquiries can be directed to the corresponding author.

Author contributions

JL and ZS write the manuscript. CY does the experimental design. BL and JR make the sample. MX draw the figures.

Funding

We would like to express appreciation to the following financial support. The National Natural Science Foundation of China, grant number 41972177, 41872169, 42172189; the Postdoctoral Science Foundation China, grant number 2018M642747; tackling key scientific and technological problems in Henan Province, grant number, 222102320346; the National Natural Science Foundation of Henan province, grant number 202300410099.

Conflict of interest

Author CY was employed by Henan Energy and Chemical Industry Group Research Institute Co., Ltd.

The remaining authors declare that the research was conducted in the absence of any commercial or financial relationships that could be construed as a potential conflict of interest.

Publisher's note

References

Bai, X., Wang, D. K., and Tian, F. C. (2021). Permeability model of damaged coal under triaxial stress loading-unloading. *Chin. J. Rock Mech. Eng.* 40 (08), 1536. doi:10.13722/j.cnki.jrme.2021.0053

Barnett, S. B., Flottmann, T., and Paul, P. K. (2015). Influence of basement structures on *in-situ* stresses over the Surat Basin, southeast Queensland. *J. Geophys. Res. Solid Earth* 120, 1. doi:10.1002/2015JB011964

Chao, J. K., Yu, M. G., Chu, T. X., Han, X., Teng, F., and Li, P. (2019). Evolution of broken coal permeability under the condition of stress, temperature, moisture content, and pore pressure. *Rock Mech. Rock Eng.* 52 (8), 2803–2814. doi:10.1007/s00603-019-01873-x

Cheng, X. Z., Chen, L. J., Luan, H. J., Zhang, J., and Jiang, Y. (2022). Why coal permeability changes under unconstrained displacement boundary conditions: Considering damage effects. *J. Nat. Gas Sci. Eng.* 105, 104702. doi:10.1016/j.jngse.2022.104702

Cheng, Y. P., Liu, H. Y., Guo, P. K., et al. (2014). A theoretical model and evolution characteristic of mining-enhanced permeability in deeper gassy coal seam. *J. China Coal Soc.* 39 (08), 1650. doi:10.13225/j.cnki.jccs.2014.9028

Connell, L. D., Lu, M., and Pan, Z. J. (2010). An analytical coal permeability model for tri-axial strain and stress conditions. *Int. J. Coal Geol.* 84 (2), 103–114. doi:10.1016/j.coal.2010.08.011

Guo, J. N., Liu, J. F., Li, Q., Xu, C., Chen, Z., and Huang, B. (2019). Variation law of coal permeability under cyclic loading and unloading. *Therm. Sci.* 23 (3), 1487–1494. doi:10.2298/tsci180907215g

Jiang, C. B., Wei, A. D., and Chen, Y. F. (2020). Experimental study of mechanical and permeability characteristics of raw coal under loading stress condition. *Saf. Coal Mines* 51 (02), 5. doi:10.13347/j.cnki.mkaq.2020.02.003

Ju, W., Wang, S. Y., and Jiang, B. (2022). Characteristics of present-day *in-situ* stress field and the Permian coal reservoir permeability in the eastern Yunnan and Western Guizhou regions. *Coal Sci. Technol.* 50 (2), 179. doi:10.13199/j.cnki.cst.2021-0169

Li, B. B, B. B., Wang, B., and Yang, K. (2020). Coal seepage mechanism effeeted by stress and temperature. *J. China Univ. Min. Technol.* 49 (05), 844. doi:10.13247/j.cnki.jcumt.001183

Li, H. G, H. G., Gao, B. B., and Wang, H. L. (2020). Numerical simulation on change of equivalent permeability of coal rock under different stress ratios. *Saf. Coal Mines* 51 (1), 195. doi:10.13347/j.cnki.mkaq.2020.11.041

Li, J. Q, J. Q., Zhou, J. H., and Huang, H. X. (2020). Study on coal rock permeability characteristics under pore pressure-stress coupling. *Coal Technol.* 39 (11), 27. doi:10.13301/j.cnki.ct.2020.11.008

Lin, F. J., Huang, G. L., Jiang, D. Y., He, Y., and Fan, J. (2022). Experimental study on coal permeability and damage evolution under the seepage-stress coupling. *Front. Earth Sci. (Lausanne).* 10, 847392. doi:10.3389/feart.2022.847392

Liu, H. H., Yu, B., Lin, B. Q., Li, Q., Mou, J., and Wang, X. (2022). Coupled effective stress and internal stress for modeling coal permeability. *Fuel* 323, 124411. doi:10.1016/j.fuel.2022.124411

Liu, Z. D., Lin, X. S., Wang, Z. Y., Zhang, Z., Chen, R., and Wang, L. (2022). Modeling and experimental study on methane diffusivity in coal mass under *in-situ* high stress conditions: A better understanding of gas extraction. *Fuel* 321, 124078. doi:10.1016/j.fuel.2022.124078

Luo, N., Suo, Y. C., Fan, X. R., Yuan, Y., Zhai, C., and Sun, W. (2022). Research on confining pressure effect of pore structure of coal-rich in coalbed methane under cyclic impact. *Energy Rep.* 8, 7336–7348. doi:10.1016/j.egyr.2022.05.238

Lv, R. S., Xue, J., Zhang, Z., Ma, X., Li, B., and Zhu, Y. (2022). Experimental study on permeability and stress sensitivity of different lithological surrounding rock combinations. *Front. Earth Sci. (Lausanne).* 9, 762106. doi:10.3389/feart.2021.762106

Meng, Y., and Li, Z. P. (2017). Triaxial experiments on adsorption deformation and permeability of different sorbing gases in anthracite coal. *J. Nat. Gas Sci. Eng.* 46, 59–70. doi:10.1016/j.jngse.2017.07.016

Meng, Z. P., Zhang, P., and Tian, Y. D. (2020). Experimental analysis of stress-strain, permeability and acoustic emission of coal reservoir under different confining pressures. *J. China Coal Soc.* 45 (7), 2544. doi:10.13225/j.cnki.jccs.DZ20.0479

Rong, T. L., Zhou, H. W., and Wang, L. J. (2018). A damage-based permeability models of deep coal under mining disturbance. *Rock Soil Mech.* 39 (11), 3983. doi:10.16285/j.rsm.2018.0787

Shi, X. H., Pan, J. N., and Hou, Q. L. (2018). Micrometer-scale fractures in coal related to coal rank based on micro-CT scanning and fractal theory. *Fuel* 212, 162–172. doi:10.1016/j.fuel.2017.09.115

Sun, G. Z., Guo, B. B., and Wang, G. Z. (2016). Experimental study on permeability to variable axial pressure and confining pressure of two kinds of coal sample. *Sci. Technol. Eng.* 16 (14), 132. doi:10.13718/j.cnki.xdzk.2019.12.016

Tatyana, V., Andrey, K., Akhmed, I., Doroshkevich, A., Ludzik, K., and Chudoba, D. M. (2022). Permeability of a coal seam with respect to fractal features of pore space of fossil coals. *Fuel* 329, 125113. doi:10.1016/j.fuel.2022.125113

Wang, D. K., Peng, M., and Fu, Q. C. (2016). Evolution and numerical simulation of coal permeability during gas drainage in coal seams. *Chin. J. Rock Mech. Eng.* 35 (04), 704. doi:10.13722/j.cnki.jrme.2015.0931

Wang, G., Wei, L. Y., and Wei, X. (2020). Permeability evolution of compacted clay during triaxial compression. *Rock Soil Mech.* 41 (01), 32. doi:10.16285/j.rsm.2018.2135

Wang, K., Guo, Y. Y., and Xu, H. (2021). Deformation and permeability evolution of coal during axial stress cyclic loading and unloading: An experimental study. *Geomechanics Eng.* 24 (6), 519. doi:10.12989/gae.2021.24.6.519

Wang, Z. W., Qin, Y., Shen, J., Li, T., Zhang, X., and Cai, Y. (2022). A novel permeability prediction model for coal based on dynamic transformation of pores in multiple scales. *Energy* 257, 124710. doi:10.1016/j.energy.2022.124710

Wang, Z. Z., Pan, J. N., and Hou, Q. L. (2018). Anisotropic characteristics of low-rank coal fractures in the Fukang mining area, China. *Fuel* 211, 182–193. doi:10.1016/j.fuel.2017.09.067

Xie, H. P., Zhang, Z. T., and Gao, F. (2016). Stress-fracture-seepage field behavior of coal under different mining layouts. *J. China Coal Soc.* 41 (10), 2405. doi:10.13225/j.cnki.jccs.2016.1393

Xue, J. H., Li, Y. H., and Li, H. B. (2021). Experimental study on change mechanism of coal and rock permeability under total stress and strain condition. *Saf. Coal Mines* 52 (02), 33. doi:10.13347/j.cnki.mkaq.2021.02.008

Xue, Y., Gao, F., and Gao, Y. N. (2017). Research on mining-induced permeability evolution model of damaged coal in post-peak stage. *J. China Univ. Min. Technol.* 46 (03), 521. doi:10.13247/j.cnki.jcumt.000681

Xue, Y. G., Zhang, D. M., and Yang, Y. S. (2020). Permeability analysis of gassy raw coal under three stresses. *Min. Saf. Environ. Prot.* 47 (03), 22. doi:10.19835/j.issn.1008-4495.2020.03.005

Yan, Z. M., Wang, K., Zang, J., Wang, C., and Liu, A. (2019). Anisotropic coal permeability and its stress sensitivity. *Int. J. Min. Sci. Technol.* 29 (3), 507–511. doi:10.1016/j.ijmst.2018.10.005

Zhao, Y. X., Cao, B., and Zhang, T. (2018). Experimental study on influences of permeability of axial pressures and penetrative pressures on broken rocks. *J. Min. Sci. Technol.* 3 (05), 434. doi:10.19606/j.cnki.jmst.2018.05.003

Zhou, H. W., Rong, T. L., and Mou, R. Y. (2019). Development in modeling approaches to mining-induced permeability of coals. *J. China Coal Soc.* 44 (01), 221. doi:10.13225/j.cnki.jccs.2018.5029

Zhu, J., Wang, Q., and Tang, J. (2021). Evolution characteristics of strain and permeability of coal samples under loading and unloading conditions. *J. China Coal Soc.* 46 (04), 1203. doi:10.13225/j.cnki.jccs.dy20.0280